UNCERTAINTIES IN KINETICS PARAMETERS OF NATURAL-URANIUM-FUELLED CANDU CORES INTRODUCED BY LATTICE HOMOGENIZATION AND GROUP CONDENSATION

E. Nichita[1], D. Serghiuta[2] and S. Podobed[2]
[1] University of Ontario Institute of Technology, Oshawa, Ontario, Canada
[2] Canadian Nuclear Safety Commission, Ottawa, Ontario, Canada

Abstract

In the Canadian Nuclear Industry, safety analysis-related reactor kinetics calculations are performed almost exclusively using the Improved Quasistatic (IQS) flux factorization method [1, 2]. The IQS method relies on calculating effective point kinetics parameters using adjoint-weighted integrals. The accuracy of the adjoint representation influences the accuracy of the effective kinetics parameters. The work presented here evaluates the effect of homogenization and group condensation on the calculated effective kinetics parameters of a Natural-Uranium-fuelled CANDU lattice as a function of burnup. Results show that, by using a two-group lattice-homogenized adjoint, the effective delayed neutron fraction is consistently overestimated by approximately 5% over a burnup range between 0 kWd/kg and 8000 kWd/kg. The effective neutron generation time is underestimated by 0.4% at 0 kWd/kg and overestimated by 1.3% at 8000 kWd/kg.

1. Introduction

Modern analysis of nuclear reactor transients uses space-time reactor kinetics methods [1]. There are several methods in use, such as direct methods, flux factorization methods and modal methods [1, 2]. The flux factorization methods can be subdivided, in inverse order of accuracy into Improved quasistatic (IQS) [3], quasistatic, adiabatic, and point kinetics [1, 2, 3]. Of these the direct and IQS methods can yield near-exact results, provided a sufficiently small time step is used [3, 4]. In the Canadian Nuclear Industry, safety analysis calculations use almost exclusively the IQS method. All methods based on flux separation rely on calculating effective point kinetics parameters which dominate the time behavior of the flux. The spatial and energy dependence can be treated with different degrees of accuracy. Because the core reactivity, effective delayed neutron fraction and generation time depend on the flux shape, approximations made in the flux shape influence the accuracy of these essential kinetics parameters. To reduce the influence of inaccuracies in the flux shape, the effective kinetics parameters are calculated using weighted integrals instead of simple integrals. The weight is chosen such that reactivity, arguably the most important of the parameters, is as insensitive as possible to small variations in the flux shape. To achieve this, the flux adjoint is used as a weighting function.

Of course, routine full-core calculations are never performed using detailed geometrical models and transport theory, but rather using a node-homogenized (cell-homogenized) model and two-group diffusion theory. This approximation will, of course, be reflected in the accuracy of the flux shape and, consequently that of the effective kinetics parameters. In particular, the intra-cell variation of the flux and adjoint, as well as their detailed energy dependence, is lost. The purpose of this work is to evaluate the effect of homogenization and group condensation on the effective kinetics parameters of a CANDU core and, if necessary, to suggest improvements to the current methodology for simulating neutronic transients of CANDU reactors.

2. Improved Quasistatic Method

Space-time kinetics calculations for CANDU reactors are routinely performed using the Improved Quasistatic (IQS) Method [3, 4] using a two-energy-group approximation for a cell-homogenized reactor model.

Assuming the system to be initially critical, the kinetics equations can be written in a compact form as follows [1, 2]:

$$\frac{\partial}{\partial t}\mathbf{v}^{-1}\mathbf{\Phi}(t) = -\mathbf{M}(t)\mathbf{\Phi}(t) + \mathbf{F}_p(t)\mathbf{\Phi}(t) + \sum_{k=1}^{k_{\max}} \lambda_k \boldsymbol{\xi}_k(t) \tag{1}$$

$$\frac{\partial}{\partial t}\boldsymbol{\xi}_k(t) = \mathbf{F}_{dk}(t)\mathbf{\Phi}(t) - \lambda_k \boldsymbol{\xi}_k(t) \quad k = 1,...k_{\max} \tag{2}$$

where the symbols have the following meanings:

$\mathbf{\Phi}(t)$	flux vector
$\boldsymbol{\xi}_k(t)$	precursor vector
λ_k	decay constant for delayed group k
$\mathbf{M}(t)$	loss operator
$\mathbf{F}_p(t)$	prompt production operator
$\mathbf{F}_{dk}(t)$	precursor production operator for delayed group k
$\mathbf{v}^{-1}$	inverse-speed operator

The exact expressions of the vectors and operators in eqs. (1) and (2) depend on the angle, energy and space approximations used.

The IQS method relies on factorizing the flux vector $\mathbf{\Phi}(t)$ into a scalar time-dependent amplitude function and a time-dependent shape vector which accounts for all the other variables, such as position, energy and, possibly, angle [1, 2].

$$\mathbf{\Phi}(t) = p(t)\mathbf{\Psi}(t) \tag{3}$$

The amplitude function is obtained as the scalar product between the flux vector $\mathbf{\Phi}(t)$ and an arbitrary weight vector, $\mathbf{w}$:

$$p(t) \equiv \left\langle \mathbf{w}, \mathbf{v}^{-1}\mathbf{\Phi}(t) \right\rangle \tag{4}$$

Equation (3) immediately yields the normalization condition for the shape vector:

$$\left\langle \mathbf{w}, \mathbf{v}^{-1}\boldsymbol{\Psi}(t)\right\rangle = 1 \tag{5}$$

The total production operator is defined as the sum of the prompt neutron and total precursor production operators.

$$\mathbf{F}(t) = \mathbf{F}_p(t) + \mathbf{F}_d(t) \tag{6}$$

In the above, $\mathbf{F}_d(t) = \sum_{k=1}^{k_{\max}} \mathbf{F}_{dk}(t)$. Additionally several *kinetics parameters* are defined:

dynamic reactivity

$$\rho(t) = \frac{\left\langle \mathbf{w}, \mathbf{F}(t)\boldsymbol{\Psi}(t)\right\rangle - \left\langle \mathbf{w}, \mathbf{M}(t)\boldsymbol{\Psi}(t)\right\rangle}{\left\langle \mathbf{w}, \mathbf{F}(t)\boldsymbol{\Psi}(t)\right\rangle} \tag{7}$$

generation time

$$\Lambda(t) = \frac{\left\langle \mathbf{w}, \mathbf{v}^{-1}\boldsymbol{\Psi}(t)\right\rangle}{\left\langle \mathbf{w}, \mathbf{F}(t)\boldsymbol{\Psi}(t)\right\rangle} \tag{8}$$

effective delayed neutron fraction for delayed group k

$$\beta_{eff}^{k}(t) = \frac{\left\langle \mathbf{w}, \mathbf{F}_{dk}(t)\boldsymbol{\Psi}(t)\right\rangle}{\left\langle \mathbf{w}, \mathbf{F}(t)\boldsymbol{\Psi}(t)\right\rangle} \tag{9}$$

(total) effective delayed neutron fraction

$$\beta_{eff}(t) = \sum_{k=1}^{k_{\max}} \beta_{eff}^{k}(t) \tag{10}$$

delayed-group k precursor population

$$\hat{C}_k = \left\langle \mathbf{w}, \boldsymbol{\xi}_k(t)\right\rangle \tag{11}$$

By using the above-defined kinetics parameters and writing the formal solution of equation (2) as:

$$\boldsymbol{\xi}_k(t) = \boldsymbol{\xi}_k(0)e^{-\lambda_k t} + \int_0^t e^{-\lambda_k (t-t')} p(t')\mathbf{F}_{dk}(t')\boldsymbol{\Psi}(t')dt' \tag{12}$$

the following set of three equations is obtained:

$$\frac{\dot{p}(t)}{p(t)}\mathbf{v}^{-1}\boldsymbol{\Psi}(t)+\mathbf{v}^{-1}\frac{\partial\boldsymbol{\Psi}(t)}{\partial t}=-\mathbf{M}(t)\boldsymbol{\Psi}(t)+p(t)\mathbf{F}_p(t)\boldsymbol{\Psi}(t)+$$
$$\frac{1}{p(t)}\sum_{k=1}^{k_{\max}}\lambda_k\left[\xi_k(0)e^{-\lambda_k t}+\int_0^t e^{-\lambda_k(t-t')}p(t')\mathbf{F}_{dk}(t')\boldsymbol{\Psi}(t')dt'\right] \tag{13}$$

$$\dot{p}(t)=p(t)\frac{\rho(t)-\beta_{eff}(t)}{\Lambda(t)}+\sum_{k=1}^{k_{\max}}\lambda_k\hat{C}_k(t) \tag{14}$$

$$\frac{\partial}{\partial t}\hat{C}_k(t)=p(t)\frac{\beta_{eff}^k(t)}{\Lambda(t)}-\lambda_k\hat{C}_k(t)\quad k=1,...k_{\max} \tag{15}$$

IQS alternates between solving eq. (13) and the set of eqs. (14) and (15) subject to the normalization condition (5). The time discretization scheme uses finer time steps for the amplitude function $p(t)$ which varies more rapidly with time, and coarser time steps for the shape vector $\boldsymbol{\Psi}(t)$ which varies more slowly with time.

The IQS equations (13) to (15) are completely equivalent to the original kinetics equations (1) and (2). The only approximation involved in the IQS method stems from the time discretization. As mentioned, the choice of the weight vector is also arbitrary. There are, however, other methods that rely on the factorization of the flux vector, such as the quasistatic, adiabatic and point-kinetics methods, which use approximate shape vectors, vectors that do not necessarily satisfy eq. (13). When approximate shape vectors are used, it is important to make the dynamic reactivity as insensitive to variations in the flux vector as possible. To achieve such insensitivity to the first order, it is shown [1, 2] that the adjoint of the initial steady state shape needs to be used as the weighting vector, that is:

$$\mathbf{w}={}^0\boldsymbol{\Psi}^* \tag{16}$$

where:

$$\mathbf{M}^*(0)\,{}^0\boldsymbol{\Psi}^*=\mathbf{F}^*(0)\,{}^0\boldsymbol{\Psi}^* \tag{17}$$

One method that employs an approximate shape vector is the adiabatic method where the shape vector $\boldsymbol{\Psi}(t)$ is calculated from a static eigenvalue problem at each time step [1, 2, 4]:

$$\mathbf{M}(t)\boldsymbol{\Psi}(t)=\frac{1}{k_{eff}(t)}\mathbf{F}(t)\boldsymbol{\Psi}(t) \tag{18}$$

It follows from eq. (18) and from the definition of the dynamic reactivity given by eq. (7) that, for the adiabatic method, the dynamic reactivity is equal to the static reactivity:

$$\rho(t)=1-\frac{1}{k_{eff}(t)} \tag{19}$$

3. Consequences of Homogenization and Group Condensation for the IQS Method

Because the implementation of the IQS method for CANDU reactors is currently based on a two-group cell-homogenized model, the shape vector $\hat{\mathbf{\Psi}}(t)$ is only an approximation of the one that would be obtained if a detailed lattice-level space and energy representation of the flux were used. The homogenization and group condensation performed for each lattice cell is equivalent to "freezing" the intra-cell flux shape and also the energy spectrum within each coarse energy group [5]. The "frozen" shape and energy dependence are the ones employed to generate the cell-homogenized and group-condensed cross sections. Because the intra-cell flux used for homogenization is obtained by way of a static eigenvalue calculation, the IQS method, as currently implemented, is akin to the adiabatic method as far as the intra-cell flux is concerned. It is therefore desirable to use an adjoint with a detailed intra-cell shape and spectrum for the weight vector. Using such a detailed adjoint as the weighting vector also allows larger steps for the solution of the shape vector since larger deviations can be tolerated without significantly affecting the accuracy of the dynamic reactivity. However, the current implementation of the IQS method is equivalent to using only a smooth (homogeneous) adjoint in each cell and a flat energy dependence of the adjoint within each coarse energy group. One instance in which this is immediately seen to be inadequate is the capturing of the effect of the softer energy spectrum of the delayed neutrons. In this two-group formalism all fission neutrons, both delayed and prompt, belong to the fast group, and because the adjoint weighting is only performed at the core level and in only two energy groups, the effect of the slightly lower energy of the delayed neutrons is lost. Additionally, there may also be spatial effects that are lost because the fine spatial variation of the adjoint inside each cell is ignored.

4. Model and Calculations

To investigate the effect of lattice-level homogenization and group condensation, a simple model consisting of an infinite array of lattice cells is considered. The kinetics parameters are consequently calculated for a two-dimensional CANDU lattice cell, consisting of a fuel channel and its associated moderator, with reflective boundary conditions. The space- and energy-dependent direct flux and the corresponding adjoint are calculated in a many-energy-group formalism using the collision-probability code DRAGON [6, 7].

For the multigroup collision probability approximation, where the flux is independent of angle, the flux vector employed in eqs. (1) and (2) becomes a column vector:

$$\mathbf{\Phi}(t) = \phi_{rg}(t) \tag{20}$$

and the operators used in equations (1) and (2) become matrices [7]:

$$\mathbf{M}(t)\mathbf{\Phi}(t) = \sum_{r',g'} M_{rg}^{r'g'}(t)\phi_{r'g'}(t) \tag{21}$$

$$\mathbf{F}_p(t)\mathbf{\Phi}(t) = \sum_{r',g'} F_{prg}^{r'g'}(t)\varphi_{r'g'}(t) = \sum_i \chi_{ig}^k \left(\sum_{g'=1}^{g_{\max}} \nu_p \Sigma_{firg'} \varphi_{rg'} \right) \delta_{rr'} \tag{22}$$

$$\mathbf{F}_{dk}(t)\mathbf{\Phi}(t) = \sum_{r',g'} F_{dkrg}^{r'g'}(t)\varphi_{r'g'}(t) = \sum_i \chi_{dig}^k \left(\sum_{g'=1}^{g_{\max}} \nu_d \Sigma_{firg'} \varphi_{rg'} \right) \delta_{rr'} \tag{23}$$

$$\mathbf{v}^{-1}\mathbf{\Phi}(t) = \frac{\phi_{rg}(t)}{\overline{\nu}_g} \tag{24}$$

In eqs. (20) to (24) the subscripts *i, r,* and *g* denote the fissile isotope, region and fine energy group respectively. $\delta_{rr'}$ is the Kronecker delta symbol.

The scalar product of any two column vectors $\mathbf{\Phi}$ and $\mathbf{\Psi}$ is defined as:

$$\left\langle \mathbf{\Psi}, \mathbf{\Phi} \right\rangle \equiv \sum_{rg} V_r \psi_{rg} \phi_{rg} \tag{25}$$

V_r represents the volume of region *r*. The effective delayed-neutron fraction and generation time are calculated using three different representations for the adjoint, to determine how appropriate each of them is: a detailed space and fine-group energy representation, a cell-homogenized fine-energy-group approximation and a cell-homogenized two-energy-group approximation.

Firstly, the reference many-group, heterogeneous effective delayed neutron fraction and generation time are calculated using a many-energy-group heterogeneous adjoint:

$$\beta_{eff}^{k} = \frac{\sum_{r\in fuel} V_r \sum_i \left[\left(\sum_{g=1}^{g_{\max}} {}^0\psi_{rg}^* \chi_{dig}^k \right) \left(\sum_{g'=1}^{g_{\max}} \nu_d \Sigma_{firg'} \psi_{rg'} \right) \right]}{\sum_{r\in fuel} V_r \sum_i \left[\left(\sum_{g=1}^{g_{\max}} {}^0\psi_{rg}^* \chi_{ig} \right) \left(\sum_{g'=1}^{g_{\max}} \nu\, \Sigma_{firg'} \psi_{rg'} \right) \right]} \tag{26}$$

$$\Lambda = \frac{\sum_{r\in cell} V_r \sum_{g=1}^{g_{\max}} {}^0\psi_{rg}^* \frac{1}{\overline{\nu}_g} \psi_{rg}}{\sum_{r\in fuel} V_r \sum_i \left[\left(\sum_{g=1}^{g_{\max}} {}^0\psi_{rg}^* \chi_{ig} \right) \left(\sum_{g'=1}^{g_{\max}} \nu\, \Sigma_{firg'} \psi_{rg'} \right) \right]} \tag{27}$$

Secondly, the many-group, homogeneous effective delayed-neutron fraction and generation time are calculated using an approximate fine-energy-group cell-homogenized adjoint, obtained by solving the adjoint static problem using cell-homogenized many-energy-group cross sections:

$$\overline{\beta}_{eff}^{k} = \frac{\sum_i \left[\left(\sum_{g=1}^{g_{\max}} {}^0\overline{\psi}_g^* \chi_{dig}^k \right) \left(\sum_{g'=1}^{g_{\max}} \overline{\nu_d \Sigma}_{fig'} \overline{\psi}_{g'} \right) \right]}{\sum_i \left[\left(\sum_{g=1}^{g_{\max}} {}^0\overline{\psi}_g^* \chi_{ig} \right) \left(\sum_{g'=1}^{g_{\max}} \overline{\nu\, \Sigma}_{fig'} \overline{\psi}_{g'} \right) \right]} \tag{28}$$

$$\overline{\Lambda} = \frac{\sum_i \sum_{g=1}^{g_{\max}} {}^0\overline{\psi}_g^* \frac{1}{\overline{\nu}_g} \overline{\psi}_{g'}}{\sum_i \left[\left(\sum_{g=1}^{g_{\max}} {}^0\overline{\psi}_g^* \chi_{ig} \right) \left(\sum_{g'=1}^{g_{\max}} \overline{\nu\, \Sigma}_{fig'} \overline{\psi}_{g'} \right) \right]} \tag{29}$$

In eqs. (28) and (29) $\overline{\nu\Sigma}_{fig'}$ represents the node-averaged production cross section, $\overline{\psi}_{g'}$ represents the solution to the direct homogenized problem and ${}^{0}\overline{\psi}_{g}^{*}$ denotes the solution to the adjoint homogenized problem.

Thirdly, the two-group homogeneous effective delayed-neutron fraction and generation time are calculated using a two-group cell-homogenized adjoint obtained by solving the adjoint static problem using cell-homogenized two-energy-group cross sections:

$$\hat{\beta}_{eff}^{k}=\frac{\sum_{i}\left[\left(\sum_{G=1}^{2}{}^{0}\hat{\psi}_{G}^{*}\chi_{diG}^{k}\right)\left(\sum_{G'=1}^{2}\hat{\nu}_{d}\hat{\Sigma}_{fiG'}\hat{\psi}_{G'}\right)\right]}{\sum_{i}\left[\left(\sum_{G=1}^{2}{}^{0}\hat{\psi}_{G}^{*}\chi_{iG}\right)\left(\sum_{G'=1}^{2}\hat{\nu}\,\hat{\Sigma}_{fiG'}\hat{\psi}_{G'}\right)\right]} \tag{30}$$

$$\hat{\Lambda}=\frac{\sum_{i}\sum_{G=1}^{2}{}^{0}\hat{\psi}_{G}^{*}\frac{1}{\overline{v}_{h}}\hat{\psi}_{G}}{\sum_{i}\left[\left(\sum_{G=1}^{2}{}^{0}\hat{\psi}_{G}^{*}\hat{\chi}_{iG}\right)\left(\sum_{G'=1}^{2}\hat{\nu}\,\hat{\Sigma}_{fiG'}\hat{\psi}_{G'}\right)\right]} \tag{31}$$

In eqs. (30) and (31) $\hat{\nu}\,\hat{\Sigma}_{fiG'}$ represents the node-averaged and group condensed production cross section, $\hat{\psi}_{G'}$ represents the solution to the direct homogenized and group condensed problem and ${}^{0}\hat{\psi}_{G}^{*}$ denotes the solution to the adjoint homogenized and group-condensed problem. Equations (30) and (31) are consistent with the current implementation of the IQS method, where it is the two-group cell-homogenized adjoint that is used to calculate the effective delayed neutron fraction.

Because the thermal components of both the prompt and the delayed fission spectrum are essentially zero and, consequently, the corresponding fast components are both equal to one, eq. (30) is equivalent to:

$$\hat{\beta}_{eff}^{k}=\frac{\sum_{i}\left(\sum_{G'=1}^{2}\hat{\nu}_{d}\hat{\Sigma}_{fiG'}\hat{\psi}_{G'}\right)}{\sum_{i}\left(\sum_{G'=1}^{2}\hat{\nu}\hat{\Sigma}_{fiG'}\hat{\psi}_{G'}\right)}=\frac{\sum_{r}V_{r}\sum_{i}\left(\sum_{g'=1}^{g_{\max}}\nu_{d}\Sigma_{firg'}\psi_{rg'}\right)}{\sum_{r}V_{r}\sum_{i}\left(\sum_{g'=1}^{g_{\max}}\nu\,\Sigma_{firg'}\psi_{rg'}\right)} \tag{32}$$

which is equivalent to using no lattice-level adjoint weighting at all.

Finally, the delayed neutron fractions and generation times for the two homogenized adjoint approximations are compared to the reference values obtained using the detailed heterogeneous fine-energy-group adjoint. Calculations are performed at multiple burnup steps covering the range from zero to discharge-burnup.

5. Microscopic Cross-Section Library and Delayed-Neutron Data

The WIMS-D Library Update (WLUP) 69-group microscopic cross section library is used [8]. Some of the isotopes present in the original fuel compositions do not exist in the WLUP library so

they are replaced with isotopes that exist in the library. In particular, all specific Cr, Fe, Ni and Zr isotopes are replaced with their natural-composition counterparts.

No material density adjustments are made to compensate for substituting or ignoring the aforementioned nuclides.

The delayed-neutron data is obtained from ENDF/B-VI.8 [9] using the Java-based processing code JANIS [10]. The delayed-neutron parameters are shown in Table 1.

The ENDF/B-VI.8 delayed-neutron spectra produced by JANIS use 10 keV intervals. The spectra are therefore converted to 69-group spectra consistent with the WLUP library before being used.

Table 1: Delayed-Neutron Parameters

Nuclide	ν_d	α_1	α_2	α_3	α_4	α_5	α_6
92-U-234	0.01290	0.05497	0.19640	0.18032	0.38771	0.13243	0.04818
92-U-235	0.01670	0.03501	0.18070	0.17251	0.38678	0.15858	0.06643
92-U-236	0.02320	0.03015	0.17222	0.16189	0.38414	0.17751	0.07408
92-U-237	0.03496	0.01784	0.14771	0.14446	0.38641	0.20952	0.09406
92-U-238	0.04400	0.01394	0.11280	0.13103	0.38514	0.25399	0.10310
93-Np-237	0.01081	0.03998	0.21618	0.15580	0.36330	0.16586	0.05887
93-Np-239	0.01670	0.03501	0.18070	0.17251	0.38678	0.15858	0.06643
94-Pu-238	0.00418	0.03768	0.23899	0.15773	0.35617	0.15904	0.05039
94-Pu-239	0.00645	0.03631	0.23644	0.17893	0.32667	0.17016	0.05150
94-Pu-240	0.00900	0.03197	0.25290	0.15082	0.33006	0.17954	0.05471
94-Pu-241	0.01620	0.01805	0.22430	0.14261	0.34925	0.19758	0.06821
94-Pu-242	0.01970	0.01964	0.23144	0.12561	0.32617	0.22554	0.07160
95-Am-241	0.00427	0.03552	0.25399	0.15632	0.33638	0.17239	0.04539
95-Am-242m	0.00690	0.02466	0.26589	0.15124	0.33374	0.17555	0.04892
95-Am-243	0.00795	0.02337	0.29449	0.15372	0.31477	0.16562	0.04803
96-Cm-242	0.00136	0.07628	0.28467	0.14187	0.28331	0.17633	0.03754
96-Cm-243	0.00301	0.03501	0.18070	0.17251	0.38678	0.15858	0.06643
96-Cm-244	0.01670	0.03501	0.18070	0.17251	0.38678	0.15858	0.06643

6. Results and Interpretation

The burnup-dependent total effective delayed-neutron fractions and effective generation time in the three studied adjoint-weighting approximations are shown in fig. 2 and fig. 3 respectively, together with the percent errors for the 69-group homogenized and 2-group homogenized results. (The 69-group heterogeneous results are taken as reference).

It can be seen from fig. 2 that the current methodology (2-group homogenized adjoint) overestimates the effective delayed neutron fraction by between approximately 4.5% at 0 kWd/kg and 5.5% at 8000 kWd/kg.

The effective generation time is seen to be underestimated by approximately 0.4% at 0 kWd/kg and overestimated by approximately 1.3% at 8000 kWd/kg.

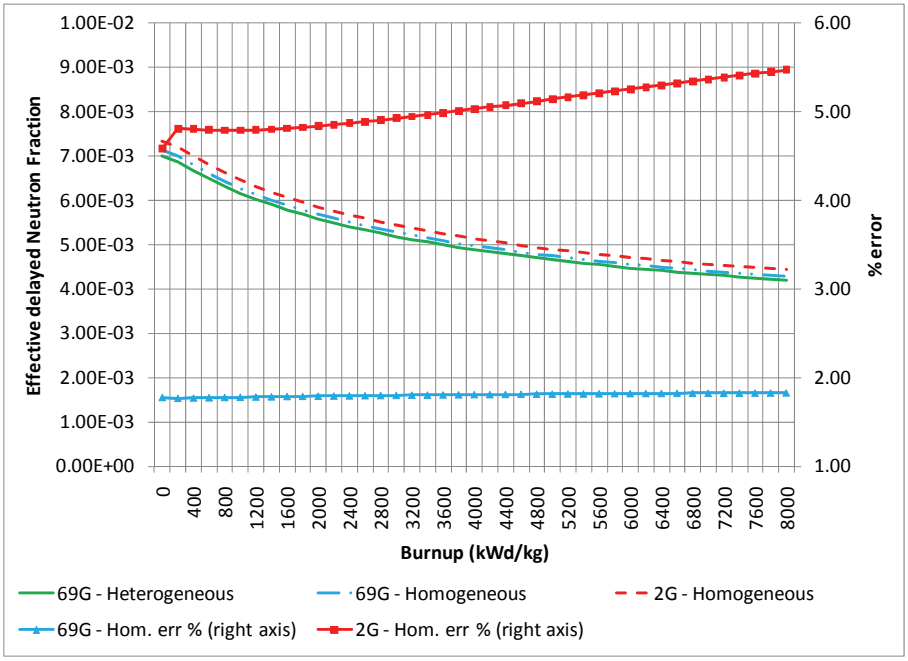

Figure 1: Effective Delayed-Neutron Fraction

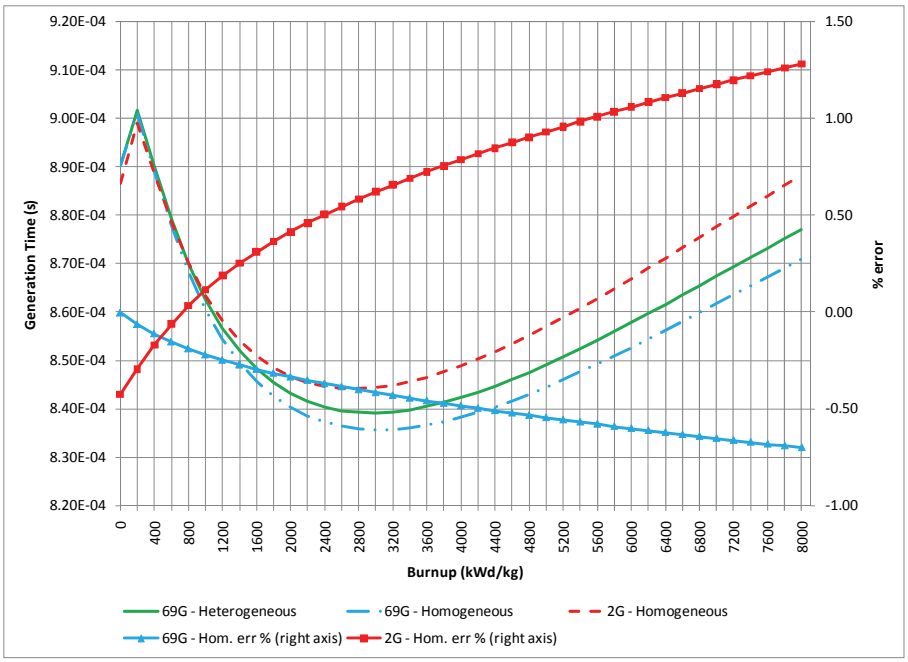

Figure 2: Effective Generation Time

If a 69-group homogenized adjoint is used, the errors are reduced and, more importantly, their variation with burnup is almost eliminated for the effective delayed-neutron fraction and greatly reduced for the effective neutron generation time. For the effective delayed-neutron fraction, the error varies from +1.8% at 0 kWd/kg to +1.9% at 8000 kWd/kg. For the effective generation time, the error varies from 0.0% at 0 kWd/kg to -0.7% at 8000 kWd/kg. The variation of the error as a

function of burnup in both cases (effective-delayed-neutron fraction and generation time) is judged to be reasonably well approximated by a straight line.

The explanation of the effect of lattice-level adjoint weighting on the effective delayed-neutron fraction can be found in ref. [11]. According to ref. [11], the adjoint is first normalized such that denominators of eqs. (26), (28) and (30), representing the three approximations of the delayed-neutron fraction, are made equal. With this normalization, the different approximations can be compared by comparing only the numerators of expressions (26), (28) and (30).

To illustrate what causes the difference in the effective delayed neutron fraction obtained using the three different approximations and given that the volume integral in the numerator is only taken over the fuel regions, it is useful to plot the adjoint for the three approximations and the delayed and total fission-source spectrum for such a fuel region.

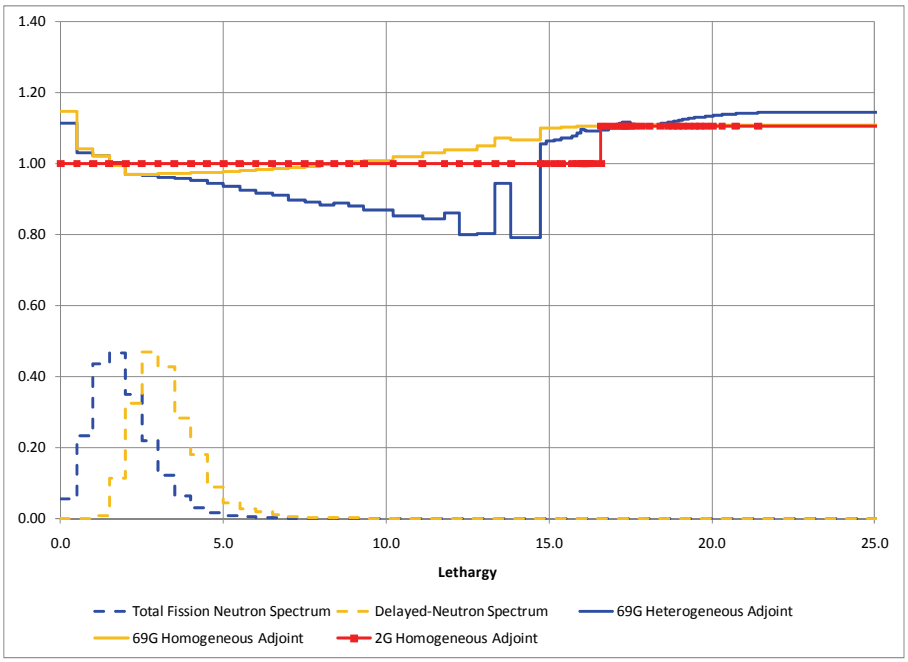

Figure 3: Adjoint Approximations at 0 kWd/kg

Figure 3 shows the normalized adjoint for a fuel region (the outer region of a fuel pin located in the outer ring), the normalized fine-group homogenized-cell adjoint and the normalized two-group homogenized-cell adjoint at zero burnup. The total fission spectrum and the spectrum of the 4th delayed group (as an example of delayed-neutron spectrum) are also plotted.

It can be seen from fig. 3 that, over the energy range where the delayed-neutron spectrum is non-zero, both the fine-group-homogenized adjoint and the two-group homogenized adjoint are different from the 69-group heterogeneous fuel adjoint. The difference is larger in the case of the two-group homogenized adjoint. The same situation exists in all fuel regions. This explains why both homogenized adjoints fail to reproduce the fine-group heterogenous-adjoint effective delayed neutron fraction and also why the fine-group homogenized adjoint yields better results than the two-group homogenized adjoint. The above argument holds true for high burnup as well, as can be seen from fig. 4.

Reference [11] also explains the minor differences in the values of the effective generation time obtained using different adjoint approximations by the fact that the three adjoints are almost equal in the moderator.

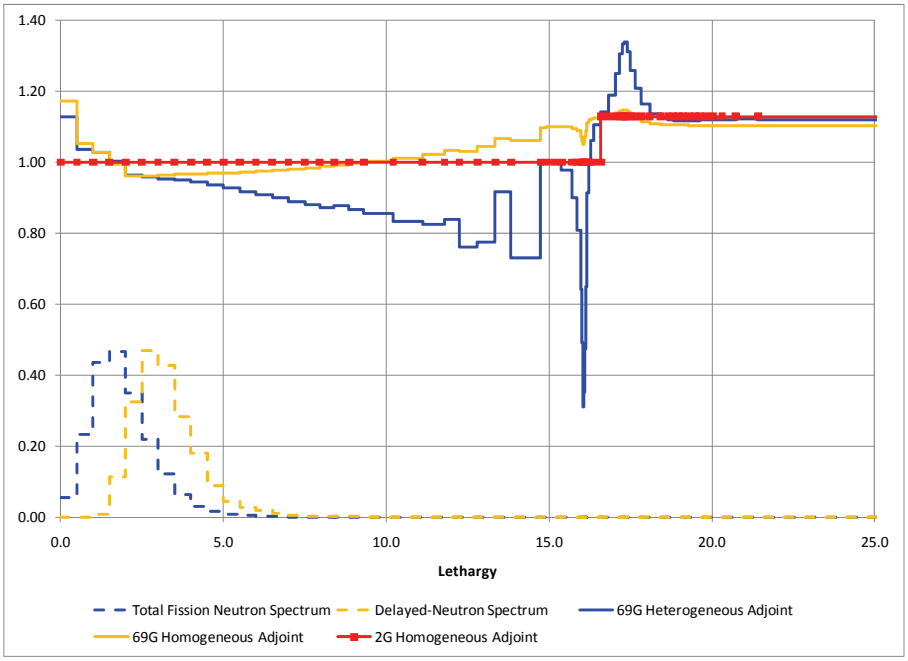

Figure 4: Adjoint Approximations at 8000 kWd/kg

Given that most of the cell neutron population is in the moderator, the near-equality of the three adjoints in the moderator leads to the near-equality of the effective generation time values.

Finally, it is noted that, because the representations of the fuel bundle used for this work may be slightly different (e.g. in spatial discretization) from the ones used in the industry, the exact values of the delayed-neutron fractions and generation time may be slightly different from those obtained with the industry models and codes. However, the differences between the values obtained using different adjoint weighting techniques are expected to be very close to what would be found with those models and codes. That is because said differences only measure the effect of different weighting techniques and the effect of weighting should be insensitive to small changes in the model.

7. Conclusion and Future Investigations

Detailed lattice-level calculations of adjoint-weighted effective delayed neutron fractions and generation time for an infinite natural-Uranium CANDU lattice were performed and results compared with those obtained following the current homogenization and group condensation methodology.

Results show that, other uncertainties notwithstanding, the current methodology (two-group lattice-homogenized adjoint weighting) introduces a positive bias of approximately 5% in the effective delayed-neutron fraction, due to a lack of weighting by a fine-group detailed-geometry adjoint at the lattice level. The bias is evident at all burnups. The use of a fine-group homogenized adjoint reduces the bias to approximately +2%, but does not eliminate it.

The bias in the effective generation time is smaller than 1.3% for all burnups. It depends on burnup, going from negative values for fresh fuel to positive values for discharge-burnup fuel, thus almost vanishing when averaged over the burnup range in the core (Absolute value of burnup-average error is less than 1%.).

Results suggest a need to address the bias in the effective delayed-neutron fraction for full-core transient analysis and for calculating "core reference" values of this parameter. Further analysis to confirm present results using different methods and codes is desirable. In particular, it is desirable to evaluate the effective delayed-neutron fraction by evaluating the change in the effective multiplication constant induced by the artificial removal of delayed neutrons. Such a calculation would be particularly valuable when performed using a high-fidelity Monte-Carlo code such as MCNP.

8. References

[1] Rozon, D., 1998. Nuclear Reactor Kinetics. Polytechnic International Press, Montreal, QC, Canada. pp. 263–286.

[2] Ott, K.O., Neuhold, R.J., 1985. Nuclear Reactor Dynamics. Am. Nucl. Soc., Lagrange Park, IL. pp. 294–299.

[3] Meneley, D.A., Ott, K.O., Wiener, E.S., 1971. Fast-reactor kinetics – the QX1 code. ANL-7769, Argonne National Laboratory, Argonne, IL, USA

[4] Ott, K.O., Meneley, D.A., 1969. Accuracy of the quasistatic treatment of spatial reactor kinetics. Nucl. Sci. Eng., 36, 402

[5] Stamm'ler, R.J.J., Abbate, M.J., 1983. Methods of steady-state reactor physics in nuclear design. Academic Press, New York, NY. pp. 337–391.

[6] Marleau, G., Hébert, A., Roy, R., 2007. A User Guide for DRAGON, Release 3.05E. Institut de génie nucléaire, Département de génie mécanique, Ecole Polytechnique de Montréal, Montréal, Canada

[7] Courau, T., Marleau, G., 2002. Adjoint and generalized adjoint flux calculations using the collision probability technique. Nucl. Sci. Eng., 141, 46.

[8] Leszczynski, F., Lopez Aldama, D., Trkov, A., editors, 2007. WIMS-D library update, IAEA, Vienna, Austria

[9] Cross Section Evaluation Working Group, 1991. ENDF/B-VI Summary Documentation. Report BNL-NCS-17541 (ENDF-201), edited by P.F. Rose, NNDC, BNL, Upton, NY, USA

[10] Soppera, N. et al., 2008. Recent upgrades to the nuclear data tool JANIS. Proceedings of the International Conference on Nuclear Data for Science and Technology, April 22-27, 2007, Nice, France. EDP Sciences

[11] Nichita, E., 2009. Effect of Lattice-Level Adjoint-Weighting on the Kinetics Parameters of CANDU Reactors. Ann. Nucl. Energy, 36, 1760-1768